QUARTERLY OF APPLIED MATHEMATICS
VOLUME LXXIV, NUMBER 4
DECEMBER 2016, PAGES 647–670
http://dx.doi.org/10.1090/qam/1443
Article electronically published on July 18, 2016

REDUCED EQUATIONS FOR THE HYDROELASTIC WAVES IN THE COCHLEA: THE SPRING MODEL

By

LYDIA PERES HARI (*Department of Mathematics, Israel Institute of Technology, Haifa 32000, Israel*),

JACOB RUBINSTEIN (*Department of Mathematics, Israel Institute of Technology, Haifa 32000, Israel*),

AND

PETER STERNBERG (*Department of Mathematics, Indiana University, Bloomington, Indiana 47405*)

Abstract. Hydroelastic waves in the cochlea are studied through modeling a passive basilar membrane as an elastic spring. A rigorous reduction of the three-dimensional equations for the fluid pressure and deflection of the basilar membrane to a one-dimensional ordinary differential equation for the pressure jump across the membrane is derived. The one-dimensional reduced model is then critically examined and limits on its validity are discussed. An approximate solution of the reduced equations is in agreement with the experimental Greenwood formula for a proper selection of elastic parameters. The model is used to compute the effect of cochlear implants on the Place Principle governing the spectral decomposition of sound by the cochlea. Numerics are also carried out to see the effect of a cochlear implant on the mechanical response of the cochlea.

1. Introduction. A main purpose of this paper is to examine reduced one-dimensional models for the fluid pressure in the cochlea and for the vibrations of the basilar membrane. Such models are ubiquitous in the literature (e.g. [1], [25], [7], [4], [11], [24], [20]). We provide the first rigorous proof of such a reduced model and then continue with a critique of the model and highlight its limitations. Another goal of the paper is to show that the empirical Greenwood function for the Place Principle of the cochlea can be derived for a general elastic model of the basilar membrane that does not contain a resonance assumption. Finally, a third goal of the paper is to use a very simple

Received December 18, 2015.
2010 *Mathematics Subject Classification.* Primary 92C10.
E-mail address: lydia@fermat.technion.ac.il
E-mail address: koby@tx.technion.ac.il
E-mail address: sternber@indiana.edu

model to compute the effect of a cochlear implant on the cochlear mechanical response to different frequencies.

The processes that take place in the cochlea are responsible for converting the incoming air vibrations impinging on the ear and converted into mechanical vibrations of the ear drum into an electrical signal in the auditory nerve. Pressure waves arrive at the cochlea after passing through the outer and middle ear. The cochlea is a curled conduit. Its precise inner structure is somewhat complicated, and we shall use here a simplified version of it. The cross section of the cochlea includes three compartments: the scala timpani, scala media, and scala vestibuli. The first and second compartments are separated by an elastic structure called the *basilar membrane* (BM). In our simpler model the scala media is omitted. The present paper models the BM as a two-dimensional sheet separating the scala timpani and the scala vestibuli that reacts locally to the force acting upon it.

The cochlea thus has two main elongated compartments. The entrance to the cochlea has two parts. The part above the BM is called the *oval window*. It is this part that is connected to the bones that transmit the signals from the ear drum. The two compartments are filled with fluid that is assumed to be incompressible. The early Von Bekesy theory for the cochlea stated that the fluid motion generates vibrations of the BM, and these vibrations in turn induce a force on tiny hair cells that are located on it. The inner dynamics of these hair cells convert the mechanical motion into chemical-electric signals that propagate then into the auditory nerve and into higher processing units in the brain. However, it was realized that the BM motion generated by the fluid motion alone, now called the *passive model*, does not suffice to activate effectively the hair cells. Therefore Gold [6] proposed the existence of a mechanism that amplifies the BM vibrations. It was realized later that there are two kinds of hair cells. The inner hair cells are those responsible for the generation of the electrical signal transmitted into the auditory nerve, while the outer hair cells form an *active* component of the cochlea, and they generate via contraction and expansion additional force on the BM.

An important well-known property of the auditory system is the decomposition of the incoming waves into their spectral components. This is achieved by an unusual property of the cochlea: the BM is not a uniform body. Rather, its elastic properties vary along the longitudinal direction. Moreover, the cochlea's thickness decreases from its base to its apex, while the BM width increases in this direction. These variations give rise to the *Place Principle*: Each wave propagating along the cochlea achieves its maximum at a position that depends on the wave's frequency. Thus, high frequency waves reach their peak near the cochlea base, while low frequency waves reach their peak closer to the cochlea apex. Indeed, one of our goals is to derive via a mathematical model an experimental formula due to Greenwood that expresses the location $\bar{x}(\omega)$ where a wave of frequency ω achieves its maximal amplitude.

Many mathematical models have been proposed for the cochlea over the years, and we do not attempt to review all of them. First, there are models for the passive cochlea. Some researchers used dimensionally reduced models from the start [11]. Other authors formally derived reduced models [10]. A comprehensive 3D numerical treatment is presented in [5]. The models also differ in the elastic complexity they use, ranging from a chain of springs [23], [11] to a full plate [10] or shell theory [5]. An overview of some

of the more prominent models can be found in chapter 20 of [13]. More recent works attempt to model the active mechanism. For example, we mention [20], [15], [14], and [24]. A particularly detailed discussion of the present understanding of the cochlea active mechanism is given in [2]. However, in the present paper we shall limit ourselves to the passive cochlea. Its simplicity makes the mathematical analysis more transparent. In a future publication we shall extend the analysis to an active cochlea model. However, we can already state that many key ideas in this paper, including the limited validity of the reduced model, are similar for active and passive cochlea. Incidentally, some auditory disorders are associated with the death of many outer hair cells; in this case the active mechanism is greatly reduced.

The main new feature of our work is a rigorous derivation of a reduced model for the pressure difference across the BM, including a critique of the model. In addition we compare the asymptotic solution of the reduced model to the experimental Greenwood formula for the Place Principle and show that this principle is generic as it holds for quite different BM elastic models. An additional new feature is the study of the effect of a cochlear implant on the Place Principle.

The paper is organized as follows: The elastic model and the fluid equations are presented in section 2. In section 3 we use the large aspect ratio of the cochlea to replace the three-dimensional equations for the hydroelastic waves by a much simpler ordinary differential equation for the pressure difference across the BM. This reduction from 3D to 1D is made rigorous through Theorem 3.2. This equation is analyzed in section 4, where we show that upon a suitable choice of elastic parameters, the equation implies the experimental Greenwood formula for the dispersion of waves along the cochlea. In section 5 we look carefully into the derivation of the reduced model and point out limitations on its validity. In section 6 we compare the accuracy of the reduced one-dimensional model with a numerical solution of the full equations. We then compute the effect of a cochlear implant on the mechanical response of the cochlea.

2. The cochlea model. Our first step is to straighten out the cochlea and represent it as an elongated prism:

$$0 < x < L,\ -ch(x) < y < ch(x),\ -cg(x) < z < cg(x). \tag{2.1}$$

The rest position of the BM is at the plane $z = 0$. The $O(1)$ nondimensional functions $h(x)$ and $g(x)$ express the changes in the cochlea cross sectional geometry as a function of x, and c is a positive scaling factor. In section 4 we shall write a specific model for g and h; however, the key point is that h is an increasing function, g decreases with x, and the product gh decreases as well. See Figure 1. Using this geometric simplification we neglect the effect of the cochlea coiling. It is believed in general that the coiling simply serves to store the elongated cochlea in the skull; some authors, though, argue that the coiling has a dynamical effect, essentially to enhance the low frequencies as the wave reaches the cochlea apex [16].

We assume that the cochlea is filled with a linear ideal fluid:

$$\rho\tilde{u}_t + \nabla\tilde{p} = 0,\ \ \nabla\cdot\tilde{u} = 0. \tag{2.2}$$

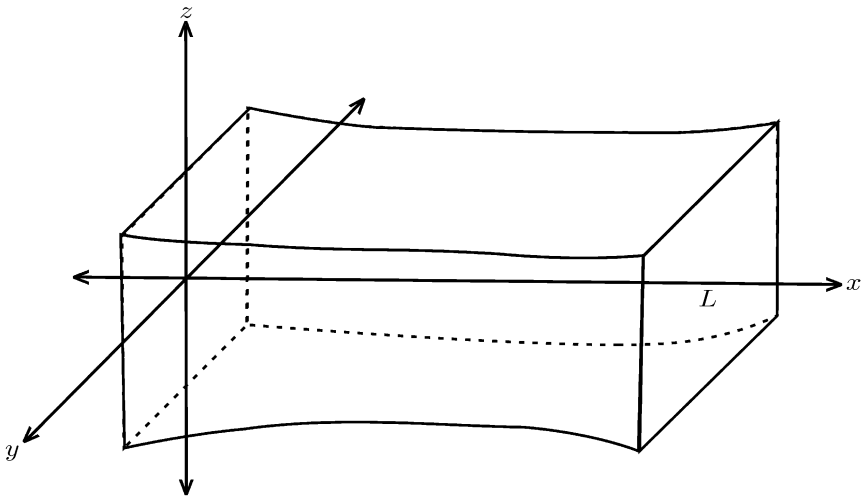

FIG. 1. The straightened-out cochlea as an elongated prism.

Here $\tilde{u}$ is the fluid velocity, $\tilde{p}$ is the pressure, and ρ is the density. The fluid equations hold in the upper and lower chambers of the cochlea. We use $\tilde{p}$ for the pressure in any of them. Later on we shall distinguish between them by using the notation $\tilde{p}^+$ and $\tilde{p}^-$. In this model we neglect the fluid viscosity. This can be justified by estimating the parameters in the problem, with further justification given in the work of Keller and Neu [12].

The boundary conditions that we use for the top, bottom and lateral sides of the cochlea are

$$\tilde{u}_\nu(x, \pm ch, z, t) = \tilde{u}_\nu(x, y, \pm cg, t) = 0 \tag{2.3}$$

where $\tilde{u}_\nu$ denotes the outer normal (to the boundary) component of the velocity. Similarly, we shall denote by ∂_ν the normal derivative operator. In addition to these conditions we write the kinematic condition

$$\tilde{u}_3(x, y, 0, t) = \tilde{w}_t(x, y, t)\hat{k}, \tag{2.4}$$

where $\tilde{w}(x, y, t)$ is the vertical deflection of the BM and where we assume that the deflection is small, and thus this boundary condition is assumed to hold at $z = 0$.

Finally, we assume that the oval window vibrates in a given way; namely, the system is driven by

$$\tilde{p}^+(0, y, z, t) = f(y, z, t) \tag{2.5}$$

for some given function f. Alternatively, one could provide a boundary condition on the velocity at the oval window. For the round window we assume that

$$\tilde{p}^-(0, y, z, t) = 0, \tag{2.6}$$

and at the apex of the cochlea we take

$$\tilde{p}^+(L, y, z, t) = \tilde{p}^-(L, y, z, t) = 0. \tag{2.7}$$

We proceed to describe our elastic model for the BM. While in reality the BM is a plate, we shall use here a simpler elastic model where we take the BM to behave like a spring with variable spring coefficient and variable friction. Thus, we write the following model for the BM vibrations:

$$m\tilde{w}_{tt} + r(x)\tilde{w}_t + \kappa(x)\tilde{w} = l. \tag{2.8}$$

Here m is the BM mass density, $r(x)$ and $\kappa(x)$ are the BM friction coefficient and spring coefficient, respectively, and l is the load on the membrane, taken here to be simply minus the pressure jump $[\tilde{p}] := \tilde{p}^+(x, y, 0, t) - \tilde{p}^-(x, y, 0, t)$. Notice that we assume that both r and κ depend upon the longitudinal direction x. Later we shall write a specific model for this dependency.

At this point we introduce typical values for the different parameters in the problem. The fluid density is taken to be $\rho = 1\ g/cm^3$. The mass density of the BM is about $m \sim 10^{-2} g/cm^2$ [22]. For the physical dimension of the cochlea we take $L \sim 35$mm, $c = 2$mm.

The BM is characterized by varying elastic parameters; in particular the spring coefficient κ decreases from the cochlea's base to its apex. A canonical model is

$$\kappa = \kappa_0 e^{-\lambda x}. \tag{2.9}$$

If the friction term $r(x)$ is momentarily neglected, the BM is expected to exhibit resonance at a position $x(\omega)$ that varies with frequency ω according to the relation $m\omega^2 = \kappa_0 e^{-\lambda x}$. This is the well-known Place Principle. While our analysis applies to a large family of BM elastic models, including the resonance model above, we shall later on show that a similar functional form for $x(\omega)$ can be derived *without* assuming resonance.

To fix ideas, and without loss of generality, we assume here the model

$$\kappa(x) = \kappa_0 e^{-\lambda x}, \quad r(x) = r_0 e^{-\lambda x}. \tag{2.10}$$

The estimates in the literature for κ and for r vary quite a bit. We select similar functional forms for κ and for r mostly for convenience. It is known [19] that the stiffness changes by a factor of about $100 - 120$ from the stapes to the apex. Therefore we expect $\lambda \sim 0.14\ \text{mm}^{-1}$. We shall later determine approximate values for the parameters r_0 and κ_0 by comparing the theory to the experimental Greenwood function.

Since we are interested mostly in the nature of the BM response to different frequencies, we assume the vibrations are driven by input f in (2.5) of the form $f = f(t) = e^{i\omega t}$ for some frequency ω. At a frequency of about 1kHz for instance, we have $\omega \sim 10^3 - 10^4\ s^{-1}$. We then anticipate that the time dependence of the pressure, velocity and displacement of the BM is similarly maintained, so we seek solutions to our problem in the form

$$\tilde{p} = p(x, y, z)e^{i\omega t},\ \tilde{u} = u(x, y, z)e^{i\omega t} \text{ and } \tilde{w} = w(x, y)e^{i\omega t}$$

for spatially dependent functions p, u and w to be determined. With these assumptions, the equations transform to

$$i\omega\rho u^{\pm} = -\nabla p^{\pm}, \quad \nabla \cdot u^{\pm} = 0 \text{ in the chambers, and} \tag{2.11}$$

$$-\omega^2 m w + i\omega r w + \kappa w = -[p] := p^+(x, y, 0) - p^-(x, y, 0) \text{ along } z = 0. \tag{2.12}$$

Since the fluid is incompressible, we can take the divergence of the first equation of (2.11), eliminate u altogether, and conclude that p is a harmonic function in each of the two chambers:

$$\Delta p^{\pm} = 0. \tag{2.13}$$

At the BM we use the continuity equation $u_3 = w_t$. This, together with the momentum equation, implies that

$$p_z^{\pm}(x, y, 0) = \omega^2 \rho w(x, y). \tag{2.14}$$

3. Rigorous derivation of a reduced model for $[p]$ and w. In this section we use the large aspect ratio of the cochlea to approximate the full model (2.11)-(2.14) above by a simpler one-dimensional model. It is useful for this purpose to scale x by L, and y, z by c. However, for simplicity of notation we retain the original notation x, y, z. We define also the small parameter $\delta = c/L$. We do not scale w and p at this point since the equations are linear in these variables. The boundary condition (2.14) now becomes

$$p_z^{\pm} = \delta L \rho \omega^2 w. \tag{3.1}$$

Solving for w in equation (2.12) and using (2.10) give

$$w = -[p] \left(-\omega^2 m + i\omega r_0 e^{-\lambda x} + \kappa_0 e^{-\lambda x} \right)^{-1}. \tag{3.2}$$

REMARK. Notice that we now use a lengthscale so that the cochlea's total length is 1, and therefore the experimental value of λ is about 4.7.

Before proceeding we seek a further simplification of the last equation, where we neglect the term $\omega^2 m$. A quick calculation indicates that $m\omega^2 \sim 10^5 - 10^6$ $dyne/cm^3$ (where we recall that a dyne is a unit of force corresponding to 1 gram-cm/sec^2), while representative values for κ_0 are around $\kappa_0 \sim 10^8 - 10^9$ $dyne/cm^3$ ([18], [22]). We shall see later on that $\omega r_0 \sim 10^8 - 10^9$ $dyne/cm^3$. Neglecting the inertia is not an essential step; its only purpose is to simplify a little the algebra below. Furthermore, in section 6 we compare the reduced model with the inertial term included and show that it has a minor effect on the results. Thus, we replace equation (3.2) by

$$w = -[p] e^{\lambda x} \left(i\omega r_0 + \kappa_0 \right)^{-1}. \tag{3.3}$$

Since κ_0 and r_0 are large and with an eye towards the asymptotic expansion we are about to carry out, we rescale them as

$$r_0 = \bar{r} L \delta^{-1}, \quad \kappa_0 = \bar{\kappa} L \delta^{-1}. \tag{3.4}$$

Therefore, equation (3.3) becomes

$$w = -\delta L^{-1} [p] e^{\lambda x} \left(i\omega \bar{r} + \bar{\kappa} \right)^{-1}. \tag{3.5}$$

Substituting this expression for w into equation (3.1) gives a closed system for $p^{\pm}$, where the boundary condition at $z = 0$ is

$$p_z^{\pm}(x, y, 0) = -\delta^2 \rho \omega^2 (iw\bar{r} + \bar{\kappa})^{-1} e^{\lambda x} [p]. \tag{3.6}$$

We now use the large aspect ratio of the cochlea to derive a reduced one-dimensional model for the pressure difference $[p]$ and the BM amplitude w. More precisely, here we will rigorously pass to the limit $\delta \to 0$ in order to obtain an ODE and appropriate

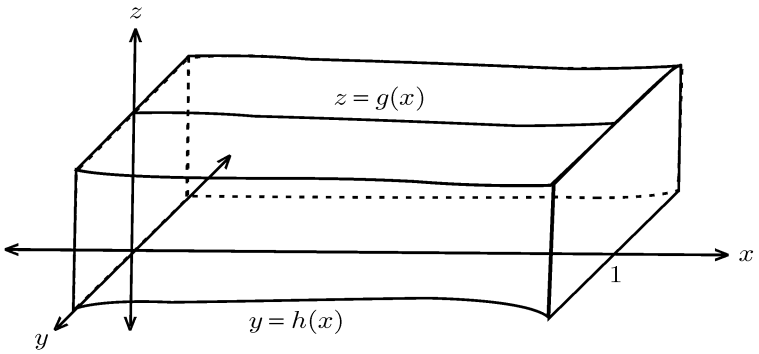

FIG. 2. The scaled domain D^+. The domain D^- consists of the even reflection of D^+ about the xy-plane in the region $\{z < 0\}$.

boundary conditions satisfied by the jump in pressure along the BM as a function of x only.

Let us first restate explicitly the 3D problem as it nows stands in the scaled variables where the upper and lower chambers above and below the BM occupy the regions

$$D^+ := \{(x, y, z) : 0 < x < 1,\ |y| < h(x),\ 0 < z < g(x)\}$$

and

$$D^- := \{(x, y, z) : 0 < x < 1,\ |y| < h(x),\ -g(x) < z < 0\}$$

respectively. See Figure 2.

For ease of notation, we will generally suppress the δ-dependence on the pressures in the upper and lower chambers and write simply p^+ and p^-, emphasizing them only as p^+_δ and p^-_δ when actually passing to the limit $\delta \to 0$. Introducing the notation $\Delta_\delta p^\pm := p^\pm_{xx} + \frac{1}{\delta^2} p^\pm_{yy} + \frac{1}{\delta^2} p^\pm_{zz}$ we then have

$$\Delta_\delta p^\pm = 0 \quad \text{in } D^\pm, \tag{3.7}$$

$$p^+(0, y, z) = 1 \text{ for } |y| < h(0),\ 0 < z < g(0), \tag{3.8}$$

$$p^+(1, y, z) = 0 \text{ for } |y| < h(1),\ 0 < z < g(1), \tag{3.9}$$

$$\mp p^+_x h'(x) + \frac{1}{\delta^2} p^+_y = 0 \text{ for } y = \pm h(x),\ 0 < z < g(x),\ 0 < x < 1, \tag{3.10}$$

$$-p^+_x g'(x) + \frac{1}{\delta^2} p^+_z = 0 \text{ for } |y| < h(x),\ z = g(x),\ 0 < x < 1, \tag{3.11}$$

$$p^-(0, y, z) = 0 \text{ for } |y| < h(0),\ -g(0) < z < 0, \tag{3.12}$$

$$p^-(1, y, z) = 0 \text{ for } |y| < h(1),\ -g(1) < z < 0, \tag{3.13}$$

$$\mp p^-_x h'(x) + \frac{1}{\delta^2} p^-_y = 0 \text{ for } y = \pm h(x),\ -g(x) < z < 0,\ 0 < x < 1, \tag{3.14}$$

$$p^-_x g'(x) + \frac{1}{\delta^2} p^-_z = 0 \text{ for } |y| < h(x),\ z = -g(x),\ 0 < x < 1, \tag{3.15}$$

$$p^\pm_z(x, y, 0) = -\delta^2 b(x)\big(p^+(x, y, 0) - p^-(x, y, 0)\big) \text{ for } |y| < h(x),\ 0 < x < 1, \tag{3.16}$$

where in (3.16) we have introduced

$$b : [0,1] \to \mathbb{C} \text{ given by } b(x) := \rho\omega^2(i\omega\bar{r} + \bar{\kappa})^{-1}e^{\lambda x}, \tag{3.17}$$

the solution in the case $k = 5$. For later use, we point out that

$$0 < \operatorname{Re} b(x) \leqslant \frac{\rho\omega^2\bar{\kappa}e^{\lambda}}{\omega^2\bar{r}^2 + \bar{\kappa}^2} \quad \text{and} \quad \operatorname{Im} b(x) \leqslant -\frac{\rho\omega^3\bar{r}}{\omega^2\bar{r}^2 + \bar{\kappa}^2} < 0. \tag{3.18}$$

In order to pass to the $\delta \to 0$ limit in this system it is necessary to obtain some a priori bounds yielding the requisite compactness along a subsequence. To this end, we establish the following:

PROPOSITION 3.1. There exists a positive constant C_0 independent of δ such that the following bound holds:

$$\begin{aligned}
&\int_{D^+} \left|p^+\right|^2 \, dx\, dy\, dz + \int_{D-} \left|p^-\right|^2 \, dx\, dy\, dz \\
&+ \int_{D^+} \left|p_x^+\right|^2 + \frac{1}{\delta^2}\left(\left|p_y^+\right|^2 + \left|p_z^+\right|^2 \right) dx\, dy\, dz + \int_{D^-} \left|p_x^-\right|^2 + \frac{1}{\delta^2}\left(\left|p_y^-\right|^2 + \left|p_z^\pm\right|^2 \right) dx\, dy\, dz \\
&+ \int_0^1 \int_{-h(x)}^{h(x)} \left|p^+(x,y,0)\right|^2 + \left|p^-(x,y,0)\right|^2 \, dy\, dx < C_0.
\end{aligned} \tag{3.19}$$

Proof. Here it will be more convenient to replace the inhomogeneity in the boundary condition (3.8) with inhomogeneities in (3.10), (3.11) and (3.16) by introducing $q^+ := p^+ - 1 + x$. Then (3.8) and (3.9) are replaced by simply

$$q^+(0,y,z) = q^+(1,y,z) = 0 \quad \text{for } |y| < h(0),\ 0 < z < g(0), \tag{3.20}$$

the boundary conditions (3.10) and (3.11) are replaced by

$$\mp h'(x)q_x^+ + \frac{1}{\delta^2}q_y^+ = \mp h'(x) \text{ for } y = \pm h(x) \text{ and } -g'(x)q_x^+ + \frac{1}{\delta^2}q_z^+ = -g'(x) \text{ for } z = g(x), \tag{3.21}$$

and the two conditions in (3.16) are replaced by

$$q_z^+(x,y,0) = p_z^-(x,y,0) = -\delta^2 b(x)\big(q^+(x,y,0) - p^-(x,y,0)\big) - \delta^2(1-x)b(x). \tag{3.22}$$

The two PDE's in (3.7) and the other boundary conditions are unchanged.

Multiplying the PDE for q^+ in (3.7) by the conjugate $(q^+)^*$ and integrating by parts over D^+, we use the boundary conditions (3.20), (3.21) and (3.22) to find that

$$\begin{aligned}
&\int_{D^+} \left|q_x^+\right|^2 + \frac{1}{\delta^2}\left(\left|q_y^+\right|^2 + \left|q_z^+\right|^2 \right) dx\, dy\, dz \\
&= \int_0^1 \int_{-h(x)}^{h(x)} \left\{ b(q^+)^*\big(q^+ - p^- + 1 - x\big) \right\}(x,y,0)\, dy\, dx + I
\end{aligned} \tag{3.23}$$

where

$$I := -\int_{\partial D^+ \cap \{y = \pm h(x)\}} h'(q^+)^* - \int_{\partial D^+ \cap \{z = g(x)\}} g'(q^+)^*. \tag{3.24}$$

Then taking the conjugate of (3.7), multiplying by q^+ and integrating we get a similar identity which we can add to (3.23) to obtain

$$\begin{aligned}&\int_{D^+} \left|q_x^+\right|^2 + \frac{1}{\delta^2}\left(\left|q_y^+\right|^2 + \left|q_z^+\right|^2\right) dx\,dy\,dz \\ &= \int_0^1 \int_{-h(x)}^{h(x)} \left\{\operatorname{Re} b \left|q^+\right|^2 - \operatorname{Re}\left[b(q^+)^* p^-\right] + (1-x)\operatorname{Re}\left[b(q^+)^*\right]\right\}(x,y,0)\,dy\,dx + \operatorname{Re} I.\end{aligned} \tag{3.25}$$

A similar manipulation of the PDE and boundary conditions for p^- gives

$$\begin{aligned}&\int_{D^-} \left|p_x^-\right|^2 + \frac{1}{\delta^2}\left(\left|p_y^-\right|^2 + \left|p_z^-\right|^2\right) dx\,dy\,dz \\ &= \int_0^1 \int_{-h(x)}^{h(x)} \left\{\operatorname{Re} b \left|p^-\right|^2 - \operatorname{Re}\left[bq^+(p^-)^*\right] + (1-x)\operatorname{Re}\left[b(p^-)^*\right]\right\}(x,y,0)\,dy\,dx.\end{aligned} \tag{3.26}$$

Addition of (3.25) and (3.26) then yields

$$\begin{aligned}&\int_{D^+} \left|q_x^+\right|^2 + \frac{1}{\delta^2}\left(\left|q_y^+\right|^2 + \left|q_z^+\right|^2\right) dx\,dy\,dz + \int_{D^-} \left|p_x^-\right|^2 + \frac{1}{\delta^2}\left(\left|p_y^-\right|^2 + \left|p_z^-\right|^2\right) dx\,dy\,dz \\ &= \int_0^1 \int_{-h(x)}^{h(x)} \left\{(\operatorname{Re} b)\left|q^+ - p^-\right|^2 + (1-x)\operatorname{Re}\left[b(q^+)^* + b(p^-)^*\right]\right\} dy\,dx + \operatorname{Re} I.\end{aligned} \tag{3.27}$$

If instead we subtract the two identities obtained in D^+ and the two identities obtained in D^- and then combine them, then we retain the imaginary counterparts to the terms arising in (3.27). This gives us

$$\begin{aligned}&\int_0^1 \int_{-h(x)}^{h(x)} (\operatorname{Im} b)\left|q^+ - p^-\right|^2 (x,y,0)\,dy\,dx \\ &\quad = \int_0^1 \int_{-h(x)}^{h(x)} (1-x)\operatorname{Im}\left[b^* q^+ + b^* p^-\right](x,y,0)\,dy\,dx + \operatorname{Im} I.\end{aligned} \tag{3.28}$$

Recalling the bounds (3.18) on the real and imaginary parts of b we can now combine (3.27) and (3.28) along with an application of Cauchy-Schwarz to conclude that

$$\begin{aligned}&\int_{D^+} \left|q_x^+\right|^2 + \frac{1}{\delta^2}\left(\left|q_y^+\right|^2 + \left|q_z^+\right|^2\right) dx\,dy\,dz + \int_{D^-} \left|p_x^-\right|^2 + \frac{1}{\delta^2}\left(\left|p_y^-\right|^2 + \left|p_z^-\right|^2\right) dx\,dy\,dz \\ &\leqslant \frac{\max \operatorname{Re} b}{\min |\operatorname{Im} b|}\left\{\int_0^1 \int_{-h(x)}^{h(x)} (1-x)\operatorname{Im}\left[b(p^-)^* + b(q^+)^*\right] dy\,dx + |\operatorname{Im} I|\right\} \\ &+ \int_0^1 \int_{-h(x)}^{h(x)} (1-x)\operatorname{Re}\left[b(q^+)^* + b(p^-)^*\right] dy\,dx + \operatorname{Re} I \\ &\leqslant C(b,g,h)\left\{\int_{\partial D^+} \left|q^+\right| + \int_{\partial D^-} \left|p^-\right|\right\} \leqslant 2C(b,g,h)\left(\int_{\partial D^+} \left|q^+\right|^2 + \int_{\partial D^-} \left|p^-\right|^2\right)^{1/2}\end{aligned} \tag{3.29}$$

where $C(b,g,h)$ is a positive constant depending on b, g, g' and h'. In the last line above we also used the definition of I given in (3.24).

At this point we appeal to the trace inequality (cf. [17], Thm. 4.2, pg. 79):

$$\begin{aligned}&\int_{\partial D^+}\left|q^+\right|^2+\int_{\partial D^-}\left|p^-\right|^2\\&\quad\leqslant C(g,h)\left(\int_{D^+}\left|q^+\right|^2+\left|\nabla q^+\right|^2\,dx\,dy\,dz+\int_{D^-}\left|p^-\right|^2+\left|\nabla p^-\right|^2\,dx\,dy\,dz\right)\end{aligned}\tag{3.30}$$

where $C(g,h)$ is a constant depending on g and h, along with the Poincaré inequality

$$\begin{aligned}\int_{D+}\left|q^+\right|^2\,dx\,dy\,dz&\leqslant C_p\int_{D^+}\left|\nabla q^+\right|^2\,dx\,dy\,dz,\\\int_{D-}\left|p^-\right|^2\,dx\,dy\,dz&\leqslant C_p\int_{D^-}\left|\nabla p^-\right|^2\,dx\,dy\,dz,\end{aligned}\tag{3.31}$$

valid for some constant $C_p>0$ in light of the homogeneous boundary conditions (3.12) and (3.20). Combining these last three inequalities we finally obtain an inequality of the form

$$\begin{aligned}&\int_{D^+}\left|q_x^+\right|^2+\frac{1}{\delta^2}\left(\left|q_y^+\right|^2+\left|q_z^+\right|^2\right)dx\,dy\,dz+\int_{D^-}\left|p_x^-\right|^2+\frac{1}{\delta^2}\left(\left|p_y^-\right|^2+\left|p_z^-\right|^2\right)dx\,dy\,dz\\&\leqslant C\left(\sqrt{\int_{D^+}\left(\left|q_x^+\right|^2+\left|q_y^+\right|^2+\left|q_z^+\right|^2\right)dx\,dy\,dz}+\sqrt{\int_{D^-}\left(\left|p_x^-\right|^2+\left|p_y^-\right|^2+\left|p_z^-\right|^2\right)dx\,dy\,dz}\right)\end{aligned}\tag{3.32}$$

for a constant $C(b,g,h)$ independent of δ. This implies a uniform bound on the left-hand side, and the bound (3.19) now follows from (3.30), (3.31) and (3.32), recalling that $p^+=q^++1-x$. □

Now we are ready to present the main result of this section, namely the reduction to a 1D model as $\delta\to 0$. Since here δ will vary, we emphasize the δ-dependence by writing $p_\delta^\pm$ and q_δ^+ for $p^\pm$ and q^+. We use the standard notation H^1 to denote the Sobolev space of square-integrable functions having square-integrable derivatives and we use the notation $\rightharpoonup$ to denote weak convergence with respect to that topology.

THEOREM 3.2. There exists an $H^1(D^+)$ function p_0^+ and an $H^1(D^-)$ function p_0^-, with $p_0^\pm=p_0^\pm(x)$ only and $p_0^+(0)=1$, $p^-(0)=0$, such that as $\delta\to 0$ one has the following convergences:

$$p_\delta^\pm\rightharpoonup p_0^\pm \text{ in } H^1(D^\pm),\tag{3.33}$$

$$p_\delta^\pm\to p_0^\pm \text{ in } L^2(D^\pm),\tag{3.34}$$

$$(p_\delta^\pm)_y\to 0 \text{ and } (p_\delta^\pm)_z\to 0 \text{ in } L^2(D^\pm),\tag{3.35}$$

$$p_\delta^\pm\to p_0^\pm \text{ in } L^2(\partial D^\pm\cap\{z=0\}) \text{ in the sense of trace.}\tag{3.36}$$

Furthermore, the functions p_0^+ and p_0^- are in fact smooth and satisfy the ODE's

$$\Big(gh(p_0^+)_x\Big)_x+hb(p_0^+-p_0^-)=0,\quad \Big(gh(p_0^-)_x\Big)_x-hb(p_0^+-p_0^-)=0\quad\text{for}\quad 0<x<1\tag{3.37}$$

along with the boundary conditions

$$p_0^+(0)=1,\ p_0^-(0)=0 \text{ and } p_0^\pm(1)=0.\tag{3.38}$$

Proof. From the estimate (3.19) we immediately see that the sequences $\{p_\delta^\pm\}$ are uniformly bounded in $H^1(D^\pm)$. Another immediate consequence of (3.19) is that $(p_\delta^\pm)_y$ and $(p_\delta^\pm)_z$ approach zero in $L^2(D^\pm)$ as $\delta \to 0$. Consequently, after passing to a subsequence $\delta_j \to 0$ we obtain (3.33)-(3.36) along that subsequence. In particular, the convergence of the traces asserted in (3.36) follows from the compactness of the trace mapping $H^1(D^\pm) \to L^2(\partial D^\pm)$; see e.g. Thm. 6.2, pg. 103, of [17].

Turning to the proof of (3.37) and (3.38), we first formulate the weak version of the PDE's and boundary conditions satisfied by $\{p_\delta^\pm\}$. Actually, for this purpose, it will again be more convenient to work with $q_\delta^+ := p_\delta^+ - 1 + x$ instead of p_δ^+. We point out that the sequence $\{q_\delta^+\}$ lies in the space of $H^1(D^+)$ functions having zero trace on $\partial D^+ \cap \big(\{x=0\} \cup \{x=1\}\big)$ and $\{p_\delta^-\}$ lies in the space of $H^1(D^-)$ functions having zero trace on $\partial D^- \cap \big(\{x=0\} \cup \{x=1\}\big)$. Furthermore, both of these spaces are closed under weak H^1 convergence, so the weak limits q_0^+ and p_0^- both have zero trace along $\{x=0\}$ and $\{x=1\}$.

Multiplying the PDE satisfied by q_δ^+ by any test function $\Psi \in H^1(D^+)$ having zero trace on $\partial D^+ \cap \big(\{x=0\} \cup \{x=1\}\big)$ and the PDE satisfied by p_δ^- by any $\Phi \in H^1(D^-)$ having zero trace on $\partial D^- \cap \big(\{x=0\} \cup \{x=1\}\big)$ and utilizing the boundary conditions, we obtain the weak formulations:

$$\int_{D^+} (q_\delta^+)_x \Psi_x + \frac{1}{\delta^2}\big((q_\delta^+)_y \Psi_y + (q_\delta^+)_z \Psi_z\big)\, dx\, dy\, dz + 2\int_0^1 \int_0^{g(x)} h'(x)\Psi\, dz\, dx$$
$$+ \int_0^1 \int_{-h(x)}^{h(x)} g'(x)\Psi\, dy\, dx - \int_0^1 \int_{-h(x)}^{h(x)} \big\{\big(b[q_\delta^+ - p_\delta^-] + (1-x)b\big)\Psi\big\}(x,y,0)\, dy\, dx = 0 \tag{3.39}$$

and

$$\int_{D^-} (p_\delta^-)_x \Phi_x + \frac{1}{\delta^2}\big((p_\delta^-)_y \Phi_y + (p_\delta^-)_z \Phi_z\big)\, dx\, dy\, dz$$
$$+ \int_0^1 \int_{-h(x)}^{h(x)} \big\{\big(b[q_\delta^+ - p_\delta^-] + (1-x)b\big)\Phi\big\}(x,y,0)\, dy\, dx = 0. \tag{3.40}$$

Applying the convergences (3.33) and (3.36) to (3.39) and (3.40) for Ψ and Φ depending only on x, we let $\delta_j \to 0$ to find that

$$\int_{D^+} (q_0^+)_x \Psi_x\, dx\, dy\, dz + 2\int_0^1 \int_0^{g(x)} h'(x)\Psi\, dz\, dx + \int_0^1 \int_{-h(x)}^{h(x)} g'(x)\Psi\, dy\, dx$$
$$- \int_0^1 \int_{-h(x)}^{h(x)} \big\{\big(b[q_0^+ - p_0^-] + (1-x)b\big)\Psi\big\}(x,y,0)\, dy\, dx = 0$$

and

$$\int_{D^-} (p_0^-)_x \Phi_x\, dx\, dy\, dz + \int_0^1 \int_{-h(x)}^{h(x)} \big\{\big(b[q_0^+ - p_0^-] + (1-x)b\big)\Phi\big\}(x,y,0)\, dy\, dx = 0.$$

In light of the lack of any y or z dependence in these integrands, the previous two equations reduce to simply

$$\int_0^1 \left\{ gh(q_0^+)'\Psi' + (gh)'\Psi - h\big(b[q_0^+ - p_0^-] + (1-x)b\big)\Psi \right\} dx = 0$$

and

$$\int_0^1 \left\{ gh(p_0^-)'\Phi' + h\big(b[q_0^+ - p_0^-] + (1-x)b\big)\Phi \right\} dx = 0$$

for all Ψ and Φ in $H_0^1(0,1)$. Then standard regularity theory implies that in fact q_0^+ and p_0^- are smooth and satisfy their respective Euler-Lagrange equations along with homogeneous Dirichlet boundary conditions at $x = 0$ and $x = 1$. Writing $p_0^+ = q_0^+ + 1 - x$ we arrive at (3.37) and (3.38).

As a final step, we will argue that the solution to (3.37)-(3.38) is unique. From this it will follow that in fact the convergences (3.33)-(3.36) hold along the full sequence $\delta \to 0$. To this end, suppose one has two solutions to the limiting problem (3.37)-(3.38), say (p_0^+, p_0^-) and $(\tilde{p}_0^+, \tilde{p}_0^-)$. Then the pair $P_0^\pm := p_0^\pm - \tilde{p}_0^\pm$ satisfies (3.37) along with homogeneous Dirichlet boundary conditions at $x = 0$ and $x = 1$ and so the function $Q := P_0^+ - P_0^-$ satisfies

$$(ghQ')' + 2hbQ = 0, \quad Q(0) = 0 = Q(1). \tag{3.41}$$

Multiplying the ODE by Q^* and integrating by parts, we find that

$$\int_0^1 2hb\,|Q|^2 - gh\,|Q'|^2\, dx = 0.$$

Similarly, taking the ODE satisfied by Q^* and multiplying it by Q, an integration by parts yields

$$\int_0^1 2hb^*\,|Q|^2 - gh\,|Q'|^2\, dx = 0.$$

Subtracting these two identities, we find that

$$\int_0^1 h(\operatorname{Im} b)\,|Q|^2\, dx = 0$$

and in light of (3.18) we conclude that $Q \equiv 0$. But then $P_0^\pm$ satisfy the ODE $(ghP_0^{\pm\,\prime})' = 0$ subject to homogeneous boundary conditions. Necessarily then, $P_0^\pm \equiv 0$, and we have uniqueness. □

REMARK. The same analysis and conclusions are valid if the boundary conditions of equation (2.7) are replaced by a homogeneous condition on the normal component of the velocity at $x = 1$. Through (2.11) this would lead to homogenous Neumann boundary conditions for the pressure

$$p_x^\pm(1, y, z) = 0 \tag{3.42}$$

replacing (3.9) and (3.13). Then the reduced model would still be given by equations (3.37), except the boundary conditions at $x = 1$ would be $(p_0^\pm)'(1) = 0$.

4. Analysis of the one-dimensional cochlea model. We now analyze the ODE for the pressure jump $P(x) := [p^0(x)]$ and conclude a formula for the location of the maximum of the BM amplitude as a function of the driving frequency ω. Using Theorem 3.2, we subtract the two equations in (3.37) to obtain a single ODE for P:

$$(ghP_x)_x + 2\rho h\omega^2\gamma^2 e^{\lambda x}P = 0, \tag{4.1}$$

where we have introduced the notation

$$\gamma^2 = \frac{1}{\bar{\kappa} + i\omega\bar{r}}. \tag{4.2}$$

For future reference we write $\gamma = \gamma_r + i\gamma_i$ and choose the square root such that

$$\gamma_r > 0 \quad \text{and} \quad \gamma_i < 0. \tag{4.3}$$

It is convenient to rewrite equation (4.1) in the form

$$P_{xx} + \frac{(gh)_x}{gh}P_x + 2\rho\omega^2\gamma^2 g^{-1}e^{\lambda x}P = 0. \tag{4.4}$$

Although the theory below is valid under general assumptions on the functions g and h, it is simplified by introducing specific functional forms for them; in particular this form will enable us to obtain the experimental Greenwood formula. Thus we set

$$g(x)h(x) = e^{-\alpha x}, \;\; g(x) = e^{-\beta x}. \tag{4.5}$$

Since the cochlea thickness varies by about a factor 2-3 from its base to the apex, and similarly the BM width grows by a smaller factor, we take the representative values $\alpha = 0.4, \beta = 0.7$.

With these assumptions equation (4.4) now takes the form

$$P_{xx} - \alpha P_x + 2\rho\omega^2\gamma^2 e^{\theta x}P = 0,$$

where $\theta = \lambda + \beta$. From now on we also take $\rho = 1$ for simplicity.

We assume that at relevant frequencies the following approximations hold:

$$\omega \gg \bar{r} \quad \text{and} \quad \omega^2 \gg \bar{\kappa}. \tag{4.6}$$

Later we shall verify the self-consistency of these assumptions. Under (4.6), one has $\omega\gamma \gg 1$ and we are justified in seeking a WKB ansatz of the form

$$P(x) \sim A(x)e^{i\omega\gamma S(x)}. \tag{4.7}$$

Grouping the leading order terms of order $\omega^2\gamma^2$ and $\omega\gamma$ respectively, we find that the phase S and amplitude A satisfy the eikonal and transport equations:

$$S_x^2 = 2e^{\theta x}, \quad \left(A^2 S_x\right)_x - \alpha A^2 S_x = 0. \tag{4.8}$$

We obtain for S:

$$S = \pm\frac{2^{3/2}}{\theta}e^{\theta x/2}. \tag{4.9}$$

For the amplitude A we find that

$$A = Ce^{\alpha x/2 - \theta x/4} \tag{4.10}$$

for some constant C.

To select the sign for S we derive a condition for forward traveling waves, namely waves that proceed from the cochlea base to its apex. For this purpose it is useful to return momentarily to the time formulation and write the pressure jump as

$$\tilde{P} := Pe^{i\omega t} = Ae^{i(\omega t+\gamma\omega S)} = Ae^{-\omega\gamma_i S}e^{i\omega(t+\gamma_r S)}. \tag{4.11}$$

Since $\gamma_r > 0$ we choose the minus sign in (4.9) to obtain a wave that moves to the right. We note here that we are neglecting the exponentially small effect of the reflected wave, but one should include it if one wants to capture the homogeneous boundary condition at $x = 1$.

Our aim now is to use the formula for P based on (4.7), (4.9) and (4.10) in the expression (3.5) for the displacement w of the BM. We obtain an expression for the amplitude of w of the form

$$|w| \sim C\exp\left(\left[\frac{\alpha}{2} - \beta + \frac{3\theta}{4}\right]x + \frac{2^{3/2}}{\theta}\gamma_i\omega e^{\theta x/2}\right) \tag{4.12}$$

for some positive constant C. We seek the x-value x_T yielding the maximal deflection of the BM as a function of the frequency ω. (Here the subscript T stands for 'theoretical'.) Maximizing the above expression and recalling the condition (4.3), we find that

$$x_T = \frac{2}{\theta}\ln\left(\frac{\alpha - 2\beta + \frac{3\theta}{2}}{2^{3/2}|\gamma_i|\omega}\right). \tag{4.13}$$

In order to compare our theoretically derived value $x_T(\omega)$ with the empirically derived Greenwood formula described below, let us now consider the regime where $\omega\bar{r} \gg \bar{k}$ so that $\gamma^2 \sim \frac{1}{i\omega\bar{r}}$ and $\gamma_i \sim -\frac{1}{\sqrt{2\omega\bar{r}}}$. Substituting this into (4.13), we find that

$$x_T \sim \frac{1}{\theta}\ln\left[\left(\frac{\alpha - 2\beta + \frac{3}{2}\theta}{2}\right)^2\frac{\bar{r}}{\omega}\right]. \tag{4.14}$$

Let us turn now to the Greenwood formula for comparison. Summarizing a body of experiments, Greenwood wrote a simple formula to fit the data for the location of the maximal BM response to a wave of a given frequency [8,9], valid over a variety of species. His formula takes the form

$$x_G = \frac{1}{a\ln 10}\ln\left[\frac{10^a A}{\omega + KA}\right], \tag{4.15}$$

where the parameters a, A and K are species-dependent. For example, in humans typical values are taken to be $a = 2.1$, $A = 165.4$ and $K = 1$. Considering (4.15) in any parameter regime where $\omega \gg KA$, one finds that

$$x_G \sim \frac{1}{a\ln 10}\ln\left[\frac{10^a A}{\omega}\right]. \tag{4.16}$$

Comparing (4.14) to (4.16) we see there is good functional agreement. Inserting for example the parameter values for humans in (4.16) one finds the prediction of the Greenwood formula in the large frequency regime to be

$$x_G \sim \frac{1}{4.8} \ln \left[\frac{20,883}{\omega} \right],$$

whereas taking the earlier mentioned values of $\lambda \approx 4.7$, $\alpha \approx 0.4$, $\beta \approx 0.7$ so that $\theta \approx 5.4$, our formula (4.14) gives

$$x_T \sim \frac{1}{5.4} \ln \left[\frac{12.6\bar{r}}{\omega} \right],$$

suggesting a value of $\bar{r} \approx 1.7 \cdot 10^3$. The value above for $\bar{r}$ is larger than what we found in the literature, where $\bar{r}$ is assumed to be about 10^2 [19], [21]. On the other hand, even for this relatively large value of $\bar{r}$ we satisfy the requirements (4.6) for say $\omega \sim 10^4$, provided $\bar{\kappa} < 10^7$, which is consistent with the values proposed in [1], [18] and [21] for the spring coefficient of the BM.

5. Critical examination of the reduced model. We proved in section 3 that the three-dimensional system of equations (3.7)-(3.16) converges to a system of ODEs. In this section we shall re-examine the validity of this result. We do not question, of course, the correctness of the mathematical analysis. However, we shall show that the analysis in section 3 and moreover the computations in section 4 are based on a certain hidden assumption. We shall examine this issue from four perspectives.

We start with a careful inspection of the estimates we used in section 3 to derive the reduced model in Theorem 3.2. The key step in the proof is a bound over the norm of the y and z derivatives of the pressure field $p(x, y, z)$. This bound is explicitly written in equation (3.19). The constant C_0 there is based on the constant $C(b, g, h)$ of equation (3.29). Therefore the bound on the partial y and z derivatives is of order $O(\delta^2 b)$. Recalling the definition of b in equation (3.17), we see that the upper bound is of $O\left(\delta^2\omega^2\gamma^2 e^{\lambda x}\right)$. Therefore, to reach the conclusion that p is to leading order independent of y and z we need the following condition to hold:

$$\delta\omega\gamma e^{\lambda x/2} \ll 1. \tag{5.1}$$

If we consider for simplicity a straight cochlea (i.e. $\alpha = \beta = 0$) and set $\delta = 0.1$, $\bar{\kappa} = 10^6$, $\bar{r} = 10^4, \lambda = 5$, then we notice that this condition indeed holds for small and intermediate values of x, but only marginally holds for $x \sim 1$.

Because of the importance of the 1D reduced model, and with an eye towards further applications of it, we now examine condition (5.1) from another, more physical, point of view. Specifically we show that condition (5.1) can be interpreted as a ratio of two inherent lengthscales in the model. First, we have the geometric lengthscale δ which characterizes the (nondimensional) thickness and width of the cochlea. Indeed, when considering reduced models in elliptic PDEs, the smallness of δ suffices to prove the validity of the reduced 1D model; these models are sometimes called quantum graphs (see e.g. [3]). However, we are considering here hydroelastic *waves*. Therefore there exists an additional scale, namely, the wavelength, which we denote here by σ. To estimate

σ we look at the WKB ansatz (4.7). The (local) wavelength is the inverse of the x derivative of the phase, namely,

$$\sigma = 1/(\omega\gamma|S_x|) = O\left(1/\omega\gamma e^{\lambda x/2}\right). \tag{5.2}$$

Therefore, to prevent variation along the y and z coordinates, and thus to obtain a one-dimensional approximation that neglects the y and z coordinates, we need that the thickness and width δ would be much smaller than the wavelength σ. The requirement $\delta \ll \sigma$ is indeed equivalent to the condition (5.1).

A third way to see the meaning of the constraint (5.1) is to compute the two limits (WKB and large aspect ratio) in a reverse order; that is, first perform a WKB analysis at the PDE level, and then expand the eikonal equation. To make the computations more transparent, and without loss of generality, we consider a simpler model than equations (3.7)-(3.17). Thus we omit the y-dependence and consider a straight cochlea, i.e. $g \equiv 1$. We start with a WKB expansion of the PDE itself by making the ansatz

$$p^{\pm}(x,z) = A^{\pm}(x,z)e^{i\Sigma(x)}. \tag{5.3}$$

Substituting this form of $p^{\pm}$ into the equations and boundary conditions and using the usual WKB assumption $\Sigma_x \gg 1$, we obtain

$$\delta^2\Sigma_x^2 A^{\pm} + A^{\pm}_{zz} = 0, \quad A^{\pm}_z(x,\pm 1) = 0, \quad A^{\pm}_z(x,0) = \delta^2 b(x)[A^{\pm}]. \tag{5.4}$$

Here we use the notation $[A^{\pm}] = A^{+}(x,0) - A^{-}(x,0)$. The equations for $A^{\pm}$ can be easily solved to give

$$A^{\pm}(x,0) = \pm\frac{\delta b[A^{\pm}]}{\Sigma_x \tanh(\delta\Sigma_x)}. \tag{5.5}$$

Therefore the eikonal equation for Σ is

$$\Sigma_x \tanh(\delta\Sigma_x) = 2b(x)\delta. \tag{5.6}$$

Hence, in the limit $\delta\Sigma_x \ll 1$, we obtain $\Sigma_x^2 = 2b(x)$, which is the same eikonal equation we derived in section 4 above. Indeed the requirement $\delta\Sigma_x \ll 1$ is equivalent to condition (5.1).

In spite of the three arguments above, showing that the 1D reduced model has limited validity near the cochlea apex, reduced models are commonly used in cochlear modeling. Indeed, it is well-known that asymptotic limits often provide very good approximations even when the 'small' parameter is not so small. To see this, we provide a fourth perspective for the reduced model by examining its validity numerically. In the next section we report on computational tests where the Place Principle curve was computed numerically. It is seen that as $\delta \to 0$, the one-dimensional solution well approximates the three-dimensional solution, except for a slight deviation just near the apex.

6. Numerical simulations and application to cochlear implants. In this section we report on numerical simulations of the underlying equations. In particular we demonstrate the accuracy of the reduced model versus the full 3D equations. We then apply the model to study the effect of a cochlear implant on the Place Principle.

We simulated equations (3.7)-(3.16) via a finite elements code. In order to concentrate on the variable elastic properties of the BM we took $g(x) = h(x) = 1$. A key test of the

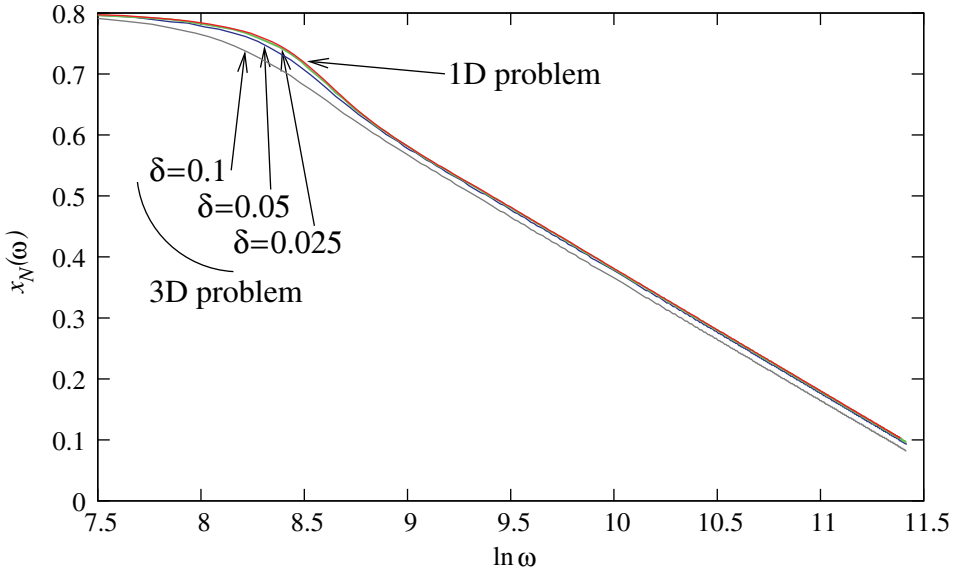

FIG. 3. Comparison of the numerical solution to the 3D model with the reduced 1D model numerical solution. The following parameters are used here: $\bar{\kappa} = 10^6,\ \bar{r} = 10^4,\ \lambda = 5$.

theory, both for the reduced model and for the WKB analysis of the preceding section, is the location $x(\omega)$ of the maximal response of the BM for a given frequency ω. The maximal deflection of the BM in the 3D model always occurs along the centerline. The location of the maximal deflection (on the centerline) for each frequency ω is denoted $x_N(\omega)$. In Figure 3 we depict the numerically computed $x_N(\omega)$ for the full 3D problem for decreasing values of the aspect ratio δ along with the *numerical* solution of the reduced 1D model. We used the parameters $\bar{\kappa} = 10^6,\ \bar{r} = 10^4,\ \lambda = 5$ in these simulations.

In section 3 we simplified the model by neglecting the inertial term. While the convergence theorem is not affected by this approximation, it was helpful in finding an explicit WKB approximation in section 4. The only effect of the inertial term is to modify the expression for γ in equation (4.2) into

$$\gamma_m^2 = \frac{1}{-m\omega^2\delta/Le^{\lambda x} + \bar{\kappa} + i\omega\bar{r}}. \tag{6.1}$$

To examine the effect of the inertial term we solved the reduced model numerically for two values of m. The results are depicted in Figure 4, where the curve of the Place Principle $x_{max}(\omega)$ is drawn (solid line) for $m = 0$ and (dashed line) for $m = 0.01$. As expected, the curves are very similar except near the cochlea apex, where the stiffness of the BM decreases substantially, and therefore the inertial term is more significant.

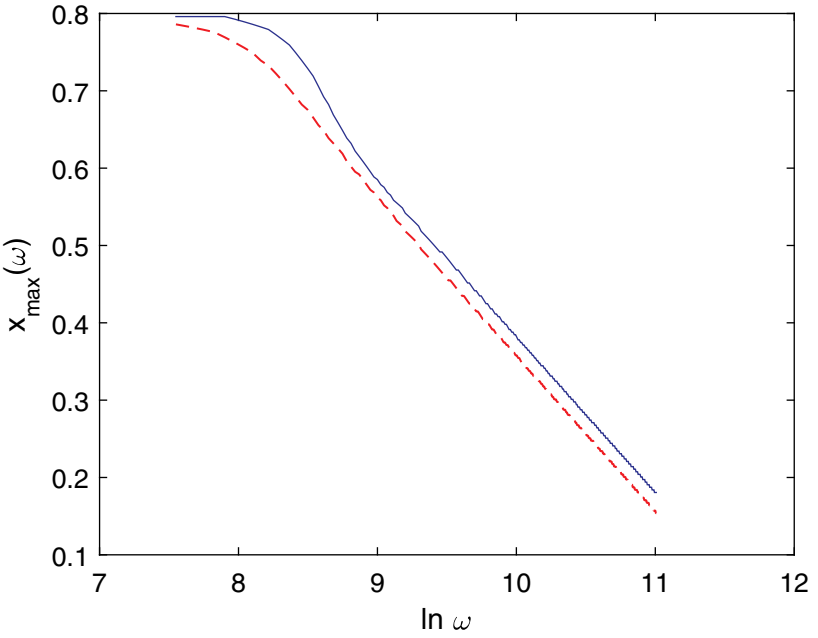

FIG. 4. Comparison of the Place Principle derived from the numerical solution of the reduced model without the inertial term, i.e. $m = 0$ (solid line), and with the inertial term $m = 0.01$ (dashed line). The following parameters were used in the simulation: $\bar{\kappa} = 10^6,\ \bar{r} = 10^4,\ \lambda = 5$.

We then compared the numerical solution of the reduced model, including the inertial term (solid line), with the WKB approximation of section 4 (dotted line), and with a Greenwood-type formula (dashed line):

$$x_G^1(\omega) = \frac{1}{5} \ln \frac{1.5 \cdot 10^5}{\omega + 10^3}. \tag{6.2}$$

The simulation was carried out with the parameters $\bar{\kappa} = 10^6,\ \bar{r} = 10^4,\ \lambda = 5$.

We see in Figure 5 a very good fit for high frequencies, which is not surprising in light of the analysis in section 4. The flattening of the curve at low frequencies in the numerical simulation is different than in the explicit function (6.2). We conjecture that this difference has to do with the crude model we use for the BM near the helicotrema, i.e. for x approaching 1.

Application to cochlear implants. When the hearing loss is associated with the cochlea malfunctioning but the auditory nerve is still functioning, a device called a *cochlear implant* can be used. An implant includes a receiver and a processor outside the

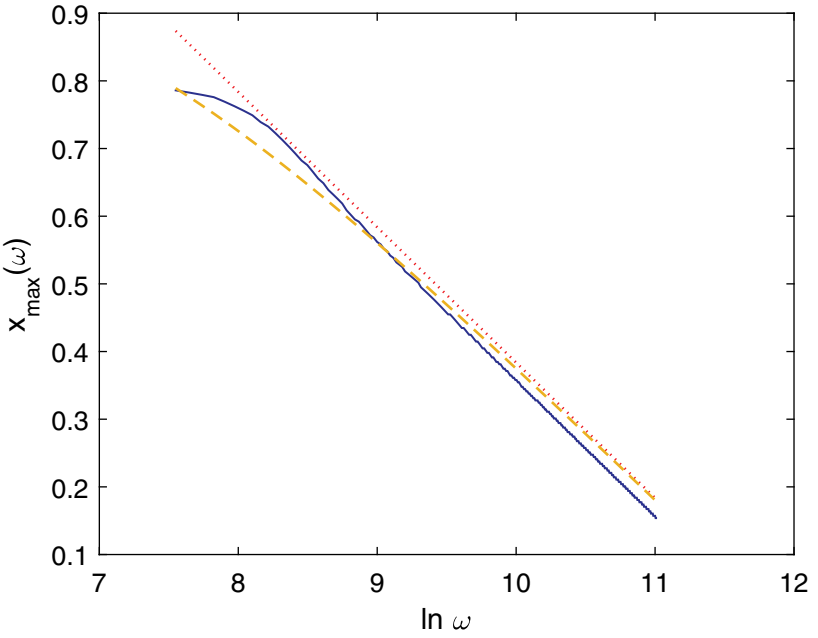

FIG. 5. Comparison of the Place Principle derived from the numerical solution of the reduced model including the inertial term (solid line), with the WKB approximation of section 4 (dotted line), and with the theoretical curve of Greenwood type given in equation (6.2) (dashed line). The following parameters were used in the simulation: $m = 0.01,\ \bar{\kappa} = 10^6,\ \bar{r} = 10^4,\ \lambda = 5.$

ear, attached to a wire that carries electrodes. The wire is inserted into the scala timpani (lower chamber) of the cochlea. Sound is decomposed by the processor into frequencies and then is transmitted to the electrodes. The electric field generated by the electrodes activates the nerves along the BM. Specific implants vary in a number of parameters. However, they are typically about 0.5mm in radius and 25mm in length, with about 24 electrodes.

Until recently cochlear implants were used for people with very severe hearing loss. However, now physicians are using them for people with mild to severe hearing loss. Therefore, prospective patients might have some rudimentary hearing. Since the electrodes are placed according to the Greenwood formula, this raises the question of how the Greenwood formula that was established for a clear cochlea is affected by the presence of the wire.

To answer this question within the present model we assume that the implant is a rigid wire positioned in the lower chamber D^-. See Figure 3 for a sketch. As a further simplification we ignore the variation in the cochlea thickness and the BM width; namely, we take $g(x) = h(x) = 1$. Thus, the modified model consists of the system (3.7)-(3.16), where now the domain D^- is replaced by

$$\bar{D}^- := D^- \backslash W, \quad W = \{(x, y, z) : 0 < x < L_w,\ y^2 + (z + 1/2)^2 \leqslant r_w^2\}, \tag{6.3}$$

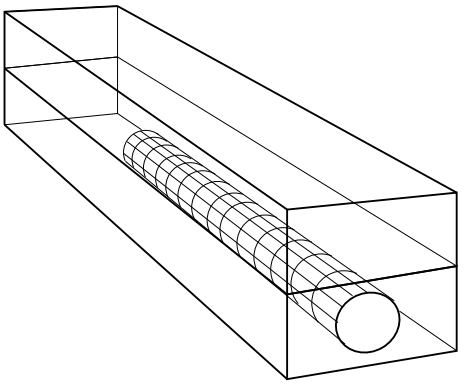

FIG. 6. A sketch of the cochlear implant model.

where L_w and r_w are the (scaled) length and radius of the implant, respectively. In addition we assume homogeneous Neumann BC for the pressure on the wire surface ∂W.

The estimates we used in section 3 to derive the reduced model (3.37) are still valid, except that D^- should be replaced everywhere by $\bar{D}^-$. It is convenient to introduce the notation $d(x)$ for the area of the cross section of the lower chamber at a point x. For instance, in the model (6.3) we have

$$d(x) = 2 - \pi r_w^2 \ \text{ for } \ 0 \leqslant x < L_W, \ \ d(x) = 2 \ \text{ for } \ L_w \leqslant x \leqslant 1.$$

Then, the reduced model (3.37) is replaced by the modified reduced model

$$p^+_{xx} + b(p^+ - p^-) = 0, \quad (d(x)p^-_x)_x - b(p^+ - p^-) = 0, \quad 0 < x < 1, \tag{6.4}$$

together with the boundary conditions (3.38). Strictly speaking, Theorem 3.2 applies as is only for smooth $d(x)$, but it is a simple matter to mollify the jump in d included in the model (6.3) or to adjust the theorem for the case where d has a jump discontinuity. In Figure 7 we compare the Place Principle for a cochlea with an implant computed with the reduced model (6.4) and with the full 3D model.

The effect of the implant is demonstrated in Figure 8, where we draw the curves $x_N(\omega)$ for the Place Principle computed for the case of clear cochlea (dashed line) and cochlea with implant (solid line). We used the parameters $\delta = 0.1$, $\bar{\kappa} = 10^6$, $\bar{r} = 10^4$, $\lambda = 5$, $L_w = 0.75$, $r_w = 0.45$. The effect of the wire is not strong. The sharp oscillation in the solid curve near $x = 0.75$ is an end effect of the wire, represented as the jump in the function $d(x)$.

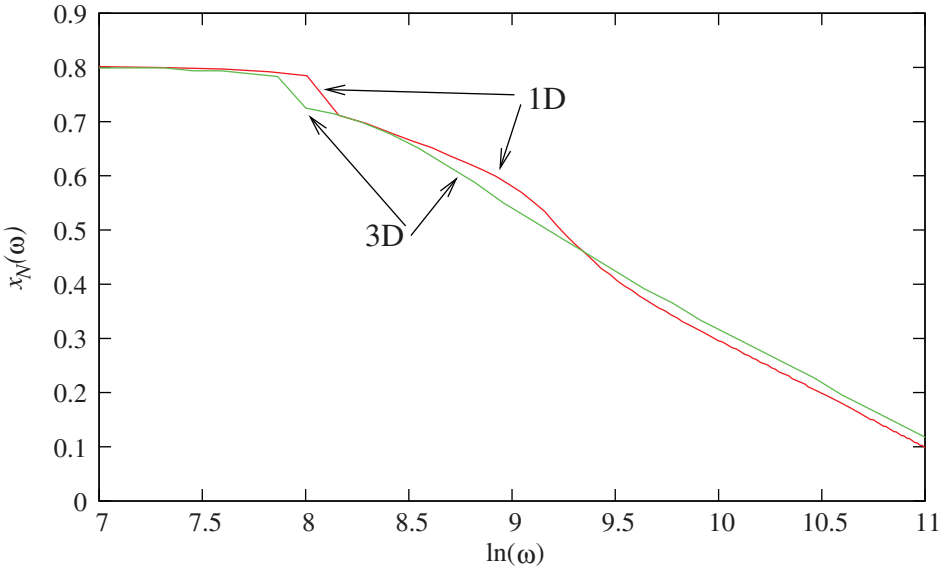

FIG. 7. The Place Principle curves $x_N(\omega)$ in the presence of a cochlear implant for the full 3D system and for the reduced model. The following parameters were used here: $\delta = 0.1$, $\bar{\kappa} = 10^6$, $\bar{r} = 10^4$, $\lambda = 5$, $L_w = 0.75$, $r_w = 0.45$.

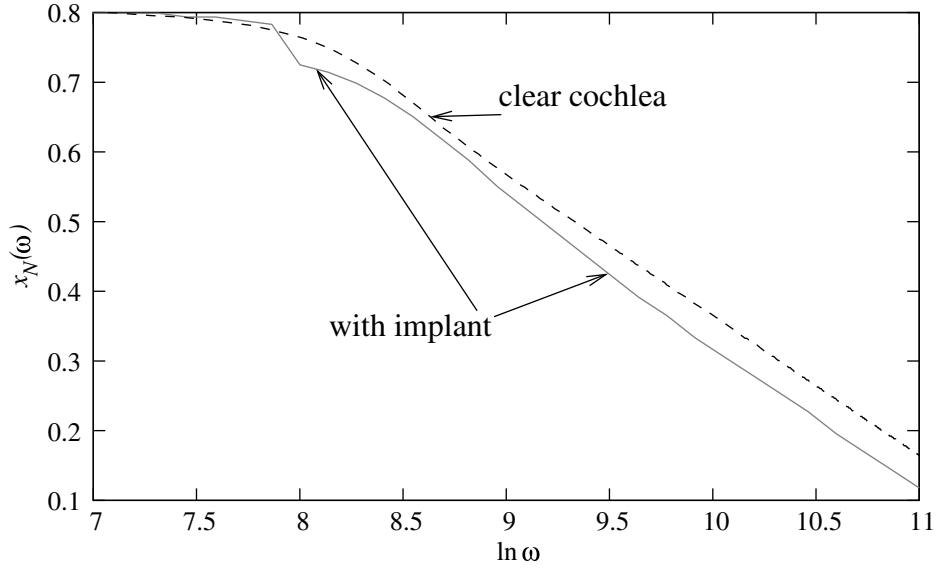

FIG. 8. The computed Place Principle curves $x_N(\omega)$ for the case of clear cochlea (dashed line) and cochlea with implant (solid line). The following parameters were used here: $\delta = 0.1$, $\bar{\kappa} = 10^6$, $\bar{r} = 10^4$, $\lambda = 5$, $L_w = 0.75$, $r_w = 0.45$.

7. Discussion. Hydroelastic waves in a passive cochlea were studied within a model where the basilar membrane is considered as a distributed spring. We used the large aspect ratio of the cochlea to reduce the full 3D problem of fluid flow in the cochlea chambers and elastic response of the BM to a single 1D differential equation for the pressure jump across the BM. This gives the first rigorous justification to a canonical model in hearing research. A key idea in the proof of Theorem 3.2 is played by the elastic dissipation term that keeps the system away from resonances.

The reduced equation was solved approximately by a WKB expansion. This solution was used to compute a formula for the Place Principle. We compared the formula to the experimental Greenwood function and showed that for a reasonable range of parameters there is good agreement, in spite of the crude model we used.

We note that the Greenwood formula was first derived through experiments with cadavers; namely, it was derived for a passive cochlea, just as in our model here. In [9], Greenwood commented on this point, saying that later experiments verified that the formula is also a good approximation for the Place Principle in active cochleas. The role of the active cochlea is to increase the response level and also to localize the response for each pure tone.

We critically examined the reduced model and pointed out that its validity is not strict, since the wavelength of hydroelastic waves might sometimes be comparable to the cochlea height and width. Nevertheless, a numerical comparison of the full 3D set of equations was shown to be in excellent agreement with the solution of the 1D model. This gives further support to the reduced model, in spite of the caveat that was described in section 5.

We applied the theory to consider the effect of a cochlear implant on the Place Principle. Again, the large aspect ratio of the cochlea and the implant were used to derive a reduced 1D model. We showed that at least in the present model the effect of the implant is quite small.

We used a number of assumptions in our analysis. The key assumption needed to justify the reduced model is of course the aspect ratio assumption $c \ll L$. However, we showed in section 5 that in fact assumption (5.1) is also required. Further assumptions we used are not essential for the main results. For instance, assumption (4.5) on the functional form of the geometric functions g, h is only needed to obtain an explicit WKB formula.

An important part of a physiological model is the selection of suitable values for the physical and chemical parameters. Like many other authors we struggled with this issue. For example, the values in the literature for the BM stiffness and friction vary over orders of magnitude. Eventually, there are four main parameters in our model. We selected the decay exponent λ in light of the experimental report that the total stiffness at the BM apex is about 120 times smaller than at its base. For the stiffness at the base and for the BM mass density we selected the most common parameters we found in the literature. The only parameter we used to fit our theoretical formula to the experimental Greenwood formula is the friction r.

The study in this paper can be upgraded in several important ways. First, as noted above, we limited ourselves here to a passive cochlea. Therefore an important way to

proceed is to extend these results to an active cochlea. There are a number of (sometimes conflicting) mathematical models for the cochlea active mechanism. We plan to pursue this direction in a future publication. However, it can already be stated that many of the key ideas used in the present analysis apply also to active cochlea models. Another direction is to replace the elastic spring model for the BM by a membrane, or even a plate, making for a more realistic model. This introduces a new difficulty, since in this case the lateral y-direction cannot be eliminated at the outset, and therefore a somewhat more delicate analysis is required, including a careful analysis of boundary layers. A further simplification that we applied here was to model the cochlea as two straight conduits. However, the coiling of the cochlea can be incorporated in the model since it does not affect the large aspect ratio. Finally, our model for the cochlear implant was crude. We are now pursuing a more accurate model where the implant is modeled as a stiff rod, pinned at one endpoint, essentially as a pendulum immersed in the cochlea fluid.

Acknowledgment. The work of the first and second authors was supported by a grant from the ISF. The work of the third author was supported by NSF grant DMS-1101290, DMS-1362879 and by a Lady Davis Fellowship at the Technion.

References

[1] J. B. Allen, Cochlear micromechanics - a mechanism for transferring mechanical to neural tuning within the cochlea, J. Acoust. Soc. Amer., 62, 930-940, 1977.
[2] J. Ashmore et al., The remarkable cochlear amplifier, Hearing Research, 266, 1-17, 2010.
[3] *Quantum graphs and their applications*, edited by Gregory Berkolaiko, Robert Carlson, Stephen A. Fulling and Peter Kuchment, Contemporary Mathematics, vol. 415, American Mathematical Society, Providence, RI, 2006. MR2279143
[4] T. Fukaawa, A model of cochlear micromechanics, Hearing Research, 113, 182-190, 1997.
[5] E. Givelberg and J. Bunn, A comprehensive three-dimensional model of the cochlea, J. Comp. Phys. 191, 377-391, 2003.
[6] T. Gold, Hearing II: The physical basis for the action of the cochlea, Proc. R. Soc. Lond. 135, 492-298, 1948.
[7] D. Geisler and C. Sang, A cochlear model using feed-forward outer hair cell forces, Hearing Research, 86, 132-146, 1995.
[8] D. D. Greenwood, Critical bandwidth and the frequency coordinates of the basilar membrane, J. Acoust. Soc. Amer., 33, 1344-1356, 1961.
[9] D. D. Greenwood, A cochlear frequency-position function for several species-29 years later, J. Acoust. Soc. Amer., 87, 2592-2605, 1990.
[10] William R. Holmes, Michael Jolly, and Jacob Rubinstein, *Hydro-elastic waves in a cochlear model: numerical simulations and an analytically reduced model*, Confluentes Math. **3** (2011), no. 3, 523–541, DOI 10.1142/S1793744211000382. MR2847242
[11] T. S. A. Jaffer, H. Kunov, and W. Wong, A model cochlear partition involving longitudinal elasticity, J. Acoust. Soc. Amer., 112, 576-589, 2002.
[12] Joseph B. Keller and John C. Neu, *Asymptotic analysis of a viscous cochlear model*, J. Acoust. Soc. Amer. **77** (1985), no. 6, 2107–2110, DOI 10.1121/1.391735. MR791675
[13] James Keener and James Sneyd, *Mathematical physiology*, Interdisciplinary Applied Mathematics, vol. 8, Springer-Verlag, New York, 1998. MR1673204
[14] Yongsam Kim and Jack Xin, *A two-dimensional nonlinear nonlocal feed-forward cochlear model and time domain computation of multitone interactions*, Multiscale Model. Simul. **4** (2005), no. 2, 664–690, DOI 10.1137/040612464. MR2162871
[15] K. M. Lim and C. R. Steele, A three-dimensional nonlinear active cochlear model analyzed by the WKB method, Hearing Research, 170, 190-205, 2002.

[16] D. Manoussaki, E. K. Dimitriadis, and R. S. Chadwick, Cochlea's graded curvature effect on low frequency waves, Phys. Rev. Lett., 96, 088701, 2006.
[17] Jindřich Nečas, *Direct methods in the theory of elliptic equations*, translated from the 1967 French original by Gerard Tronel and Alois Kufner; editorial coordination and preface by Šárka Nečasová and a contribution by Christian G. Simader, Springer Monographs in Mathematics, Springer, Heidelberg, 2012. MR3014461
[18] W. M. Siebert, Ranke revisited-a simple short wave cochlear model, J. Acoust. Soc. Amer., 56, 594-601, 1974.
[19] C. R. Steele and L. A. Taber, Comparison of WKB and finite difference calculations for a two dimensional cochlear model, J. Acoust. Soc. Amer., 65, 1001-1006, 1979.
[20] R. Szalai, K. Tsaneva-Atanasova, M. E. Homer, A. R. Champneys, H. J. Kennedy, and N. P. Cooper, *Nonlinear models of development, amplification and compression in the mammalian cochlea*, Philos. Trans. R. Soc. Lond. Ser. A Math. Phys. Eng. Sci. **369** (2011), no. 1954, 4183–4204, DOI 10.1098/rsta.2011.0192. MR2843876
[21] M. A. Viergever, A two dimensional model for the cochlea: The heuristic approach and numerical results, J. Engn. Math., 11, 11-28, 1971.
[22] M. A. Viergever, *Mechanics of the inner ear*, Thesis, Technical University Delft, 1980.
[23] J. Xin, Dispersive instability and its minimization in time-domain computation of steady-state responses of cochlear models, J. Acoust. Soc. Amer., 115, 2173-2177, 2004.
[24] Y. Yoon, S. Puria, and C. R. Steele, A cochlear model using the time-averaged Lagrangian and the push-pull mechanism in the organ of Corti, J. Mech. Mater. Struct., 4, 977-986, 2009.
[25] G. Zweig, Finding the impedance of the organ of corti, J. Acoust. Soc. Amer., 89, 1229-1254, 1991.